Available online at www.sciencedirect.com
ScienceDirect
International Journal of Impact Engineering 35 (2008) 1063–1074
INTERNATIONAL JOURNAL OF IMPACT ENGINEERING
www.elsevier.com/locate/ijimpeng

Mechanical response of metallic honeycomb sandwich panel structures to high-intensity dynamic loading

Kumar P. Dharmasena[a,*], Haydn N.G. Wadley[a], Zhenyu Xue[b], John W. Hutchinson[b]

[a]Department of Materials Science & Engineering, University of Virginia, USA
[b]Division of Engineering and Applied Sciences, Harvard University, USA

Received 9 September 2005; received in revised form 1 June 2007; accepted 3 June 2007
Available online 10 July 2007

Abstract

Explosive tests were performed in air to study the dynamic mechanical response of square honeycomb core sandwich panels made from a super-austenitic stainless steel alloy. Tests were conducted at three levels of impulse load on the sandwich panels and solid plates with the same areal density. Impulse was varied by changing the charge weight of the explosive at a constant standoff distance. At the lowest intensity load, significant front face bending and progressive cell wall buckling were observed at the center of the panel closest to the explosion source. Cell wall buckling and core densification increased as the impulse increased. An air blast simulation code was used to determine the blast loads at the front surfaces of the test panels, and these were used as inputs to finite element calculations of the dynamic response of the sandwich structure. Very good agreement was observed between the finite element model predictions of the sandwich panel front and back face displacements and the experimental observations. The model also captured many of the phenomenological details of the core deformation behavior. The honeycomb sandwich panels suffered significantly smaller back face deflections than solid plates of identical mass even though their design was far from optimal for such an application.

Keywords: Air blast testing; Blast loading; Finite element simulation; Impulse loads; Sandwich panels

1. Introduction

The need to protect structures from the high-intensity dynamic loads created by explosions has stimulated renewed interest in the mechanical response of metallic structures subjected to localized, high rate loading [1,2]. One promising approach utilizes sandwich panel concepts to disperse the mechanical impulse transmitted into structures, thereby reducing the pressure applied to a protected structure located behind the panel [1–3].

A schematic illustration of the basic concept is shown in Fig. 1. Consider a sandwich panel consisting of a pair of solid metal faces and a cellular metal core that is rigidly edge supported and an explosive charge is detonated above the system. Several groups have examined the dynamic response of sandwich structures to impulse loading [1–5]. Detailed finite element calculations using fully meshed geometries with a square honeycomb, prismatic corrugations and pyramidal truss topologies made from materials defined by their yield strength, strain hardening rate and strain rate sensitivity have been conducted. These studies indicate a complex dynamic structural response.

For near-field air blasts, a shock wave propagates from the source of the explosion to the front face and is reflected. The pressure resulting from the shock wave decays with distance (from the explosion source) and time. When the shock is incident on a rigid surface, the shock wave front undergoes a reflection. This requires the forward-moving air molecules comprising the shock wave to be brought to rest and further compressed, inducing a reflected overpressure on the wall that is of higher magnitude than the incident overpressure [6–8]. An impulse is imparted to the front face of the structure (Fig. 2a), causing it to acquire a velocity, Fig. 2b. In the acoustic limit, the pressure pulse applied to the sample front face during this process is twice

*Corresponding author.
E-mail address: Kumar@Virginia.edu (K.P. Dharmasena).

0734-743X/$ - see front matter © 2007 Elsevier Ltd. All rights reserved.
doi:10.1016/j.ijimpeng.2007.06.008

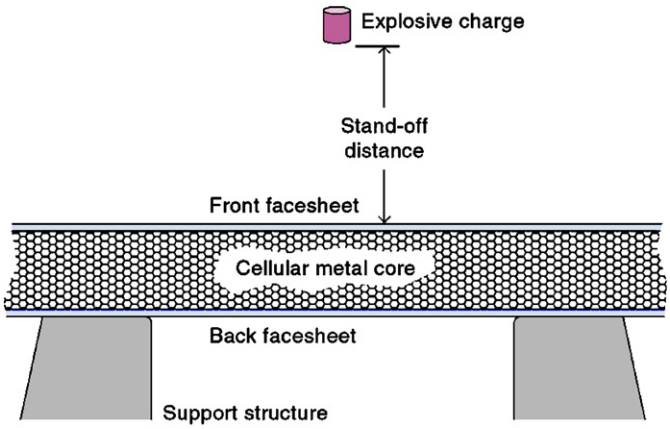

Fig. 1. Air blast mitigation concept using a sandwich panel.

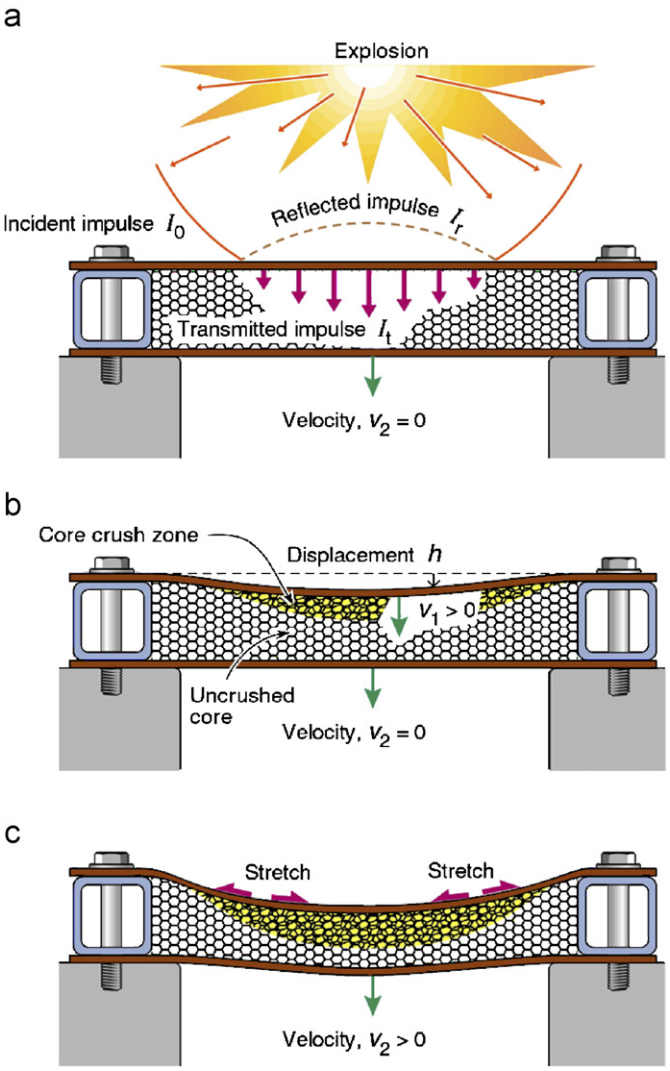

Fig. 2. Response of sandwich beams to blast loading. (a) Impulse loading (stage I); (b) core crushing (stage II); (c) panel bending (stage III).

that of the free-field shock (large stand-off distances and for weak explosions). In the near field where non-linear effects are present in the shock front, the pressure reflection coefficient can rise to a value of eight (under an ideal gas assumption). Even larger pressure reflection coefficients result when real gas effects (dissociation and ionization of the air molecules) occur in the free-field shock [6,7]. Deshpande and Fleck [9] refer to this initial phase of the blast shock–structure interaction as Stage I.

For an ideal blast with no delayed (reflected) shock arrivals (e.g. due to the ground), a front face of mass m_f will be moving at a velocity V_1 towards the back face sheet, and will have acquired its full momentum ($m_f V_1$) at the end of stage I. For sandwich panel structures, this front face motion is resisted by compression of the cellular core. A region of densified core is then created at the front face and this propagates at the core plastic wave speed towards the back face (Fig. 2b). This plastic wave speed V_p is given by

$$V_p = \sqrt{E_t/\bar{\rho}}, \tag{1}$$

where E_t is the tangent modulus of the material used to make the core structure and $\bar{\rho}$ is its relative density. V_p is typically $\sim$500 m/s for stainless steel alloys subjected to plastic strains of around 10%. It is about a tenth of the elastic wave speed of the materials used to make the structure.

Core crushing occurs at a characteristic pressure and this crushing resists the front plate movement and slows the front face motion (Stage II). For weak explosive shocks, it is possible to arrest the densification front within the core [10]. The pressure that is transmitted to the support structure is controlled by the dynamic crush strength of cellular material during densification [11]. This crush strength depends on the core relative density, cell topology and properties of the material used to make the cellular structure [12].

For large, spatially localized shock loadings, the impulse transmitted to the back face sheet can be sufficient to cause an edge-supported panel to bend. During this panel bending (Stage III), Fig. 2c, further mechanical energy dissipation occurs by a combination of core collapse and core/face sheet stretching. In a well-designed system, the restraining forces accompanying this plastic dissipation are sufficient to arrest the motion of the panel before the loads applied to the support structure exceed design objectives, or tearing of the front face plate occurs. It is important to recognize that core crushing continues to play an important role during Stage III because highly crush-resistant cores maintain a larger face sheet separation and therefore a higher panel bend resistance [13].

Efforts to implement these blast shock wave protection concepts require a detailed understanding of the dynamic structural response and core collapse mechanisms, the development of a design science that enables preferred core topologies, core relative densities and core materials to be identified, and manufacturing approaches for the materials/topologies of interest. Recent studies indicate that a square honeycomb topology with the webs aligned perpendicular to the face sheets has the highest crush resistance [14]. The dynamic response of this core to

a shock wave has been simulated using the finite element method [14]. Significant quasi-static core strength enhancements can be achieved by constructing such cores from metals with a high yield strength and tangent modulus. This causes web buckling to control the core strength and the critical strength for this buckling mode can increase by increasing the web material's tangent modulus. During dynamic loading, additional core strengthening has been predicted to occur by inertial buckling stabilization and strain rate hardening [14]. Materials with a high strength, tangent modulus and strain hardening rate are then best suited for blast wave mitigation applications. Many austenitic and super-austenitic stainless steels have a desirable combination of these properties [15].

Recent cellular manufacturing developments now enable the fabrication of many cellular metal core structures from stainless steels. These include the fabrication of triangular and square honeycombs [16], prismatic corrugations [17], lattice truss structures with pyramidal, tetrahedral, three-dimensional Kagome architectures [17,18], and lattice structures with hollow truss or wire mesh lay-ups [19]. These cellular metal cores can be attached to face sheets using transient liquid phase bonding methods to create sandwich panel structures.

Here, we describe a method for making square honeycomb sandwich cores from super-austenitic stainless steels and use it to construct large sandwich panels with a core relative density of around 5–6%. The panels were then exposed to shock waves created by close proximity air blasts and the resulting deformation and structural collapse mechanisms were characterized. The panel's distribution of mass between the top face sheet, core and bottom face sheet was around 2:1:2, somewhat different from distributions obtained from preliminary optimization studies [5]. Thicker panel faces than the optimized mass distributed design were used to deliberately avoid face sheet tearing so that the core collapse behavior under very high intensity loadings could be examined. We also tested and characterized solid plates of equivalent mass per unit area subjected to identical explosive loadings. The pressure fields applied to the panels were estimated using an air blast simulation code [8], and finite element simulations were then performed using ABAQUS/Explicit [20] to investigate the dynamic deformation sequence and the core collapse mechanisms controlling the overall response. The non-optimized sandwich panels tested here suffered significantly smaller back face deflections than their equivalent areal density solid counterparts.

2. Air blasts

When an explosive charge is detonated in air, the rapidly expanding gaseous reaction products compress the surrounding air and move it outwards with a high velocity that is initially close to the detonation velocity of the explosive (~7200 m/s). The rapid expansion of the detonation products creates a shock wave with discontinuities in pressure, density, temperature and velocity [6]. The pre- and post-shock states are described by conservation equations for mass, momentum and energy, and are collectively referred to as the Rankine–Hugoniot jump equations [6].

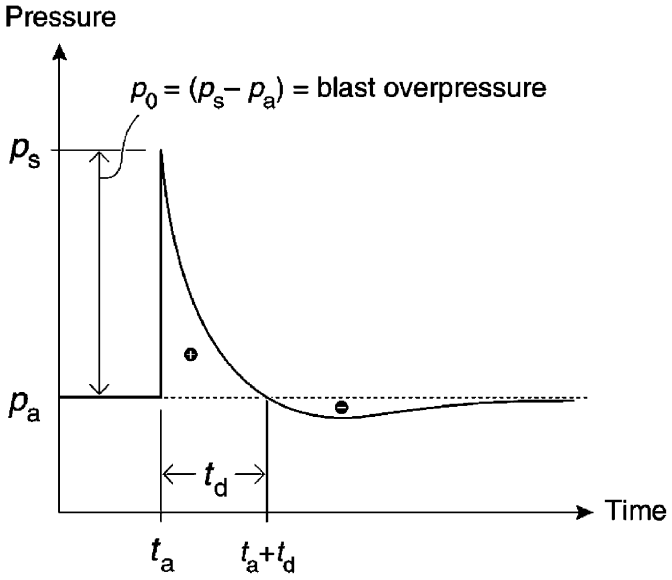

Fig. 3. Characteristic air blast pressure response.

The shock wave that travels through the air consists of highly compressed air particles that exert pressure on all surfaces they encounter. There is a discontinuous "jump" of the shock front pressure, with the pressure rising from ambient (p_a) to p_s. The pressure difference ($p_s - p_a$) is referred to as the blast overpressure (Fig. 3). At a fixed location in space, the pressure decays exponentially with time and is followed by a negative (i.e. suction) phase. An ideal blast wave pressure pulse has a very short time duration, typically measured in fractions of milliseconds. The free-field pressure–time response can be described by a modified Friedlander equation,

$$p(t) = (p_s - p_a)\left[1 - \frac{t - t_a}{t_d}\right] e^{-(t-t_a)/\theta}, \quad (2)$$

where t_a is the arrival time, t_d the time duration of the positive phase and θ the time decay constant [8].

The air blast load intensity on a target surface depends on the explosive material, the mass of the explosive (m) and the standoff distance between the explosive and the target surface (r). The free-field peak pressure of the blast wave (P) for a given explosive can be approximated by

$$P = K\left[\frac{m}{r^3}\right], \quad (3)$$

where K is an explosive material parameter [21].

When the shock wave encounters a surface, it is reflected, amplifying the incident overpressure. The magnification can be highly non-linear and depends on the incident shock strength and the angle of incidence. For a weak shock, the

resultant blast loads are doubled on reflection of the shock wave. For strong shocks, reflection coefficients of 8 have been reported assuming ideal gas conditions and up to 20 when real gas effects such as the dissociation and ionization of air molecules have been considered [6].

The impulse load (I) delivered to the structure can be calculated by the time integration of the applied pressure–time response during the positive phase:

$$I = \int_{t_a}^{t_a+t_d} p\,\mathrm{d}t, \tag{4}$$

where p is the incident pressure multiplied by the pressure reflection coefficient. The pressure and impulse loads applied to the surface of the test structures examined here were estimated using ConWep, a blast simulation code developed by the US Army Corps of Engineers [8].

3. Sandwich panel fabrication

Fig. 4(a) shows the design of the flat test panel structure used for the study. For a square honeycomb core geometry with straight webs, the core relative density is determined by the thickness of the honeycomb cell walls (t) and the spacing between the webs (l). The test panels used here are subjected to large bending loads, and it is important to create high-strength joints between the core webs and face sheets. To enable this, a small top and bottom L-shaped flange was used to ensure a larger contact area between the core webs and the face sheet.

The core relative density, $\bar{\rho}$, of the flange-modified square honeycomb can be calculated from the unit cell, Fig. 4(b).

$$\bar{\rho} = \frac{\rho_c}{\rho_s} = \frac{2t(h+2w)}{lh}, \tag{5}$$

where t is the cell wall thickness, l the cell spacing, h the core height, w the flange width, ρ_c the core density and ρ_s the parent alloy density. Recent studies have shown that sandwich core relative densities in the 3–10% range are of most interest for blast resisting structures [2]. In this study, square honeycomb core panels were designed with a core relative density of approximately 6%. These cores had a 0.76 mm web (wall) thickness, a 5 mm flange width and a cell wall spacing of 30.5 mm.

Selections of the face sheet thickness and core height were dictated by a desire to avoid face sheet rupture and the retention of the ability to compare the performance of the sandwich panel with an equivalent solid plate with the same areal density. The sandwich panel equivalent mass solid plate thickness, t_s, is given by

$$2t_f + \bar{\rho}h_c = t_s. \tag{6}$$

For the series of tests reported here, a thickness of 5 mm was used for the front and back face plates and a thickness of 51 mm for the core. With a 6% core density, the

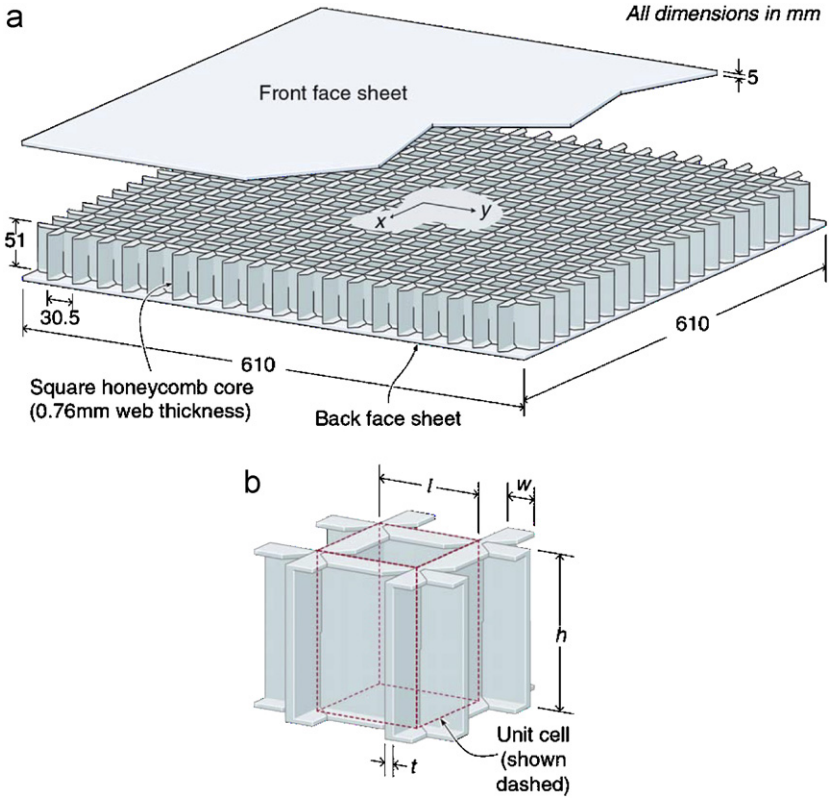

Fig. 4. Square honeycomb core sandwich panel design for air blast tests.

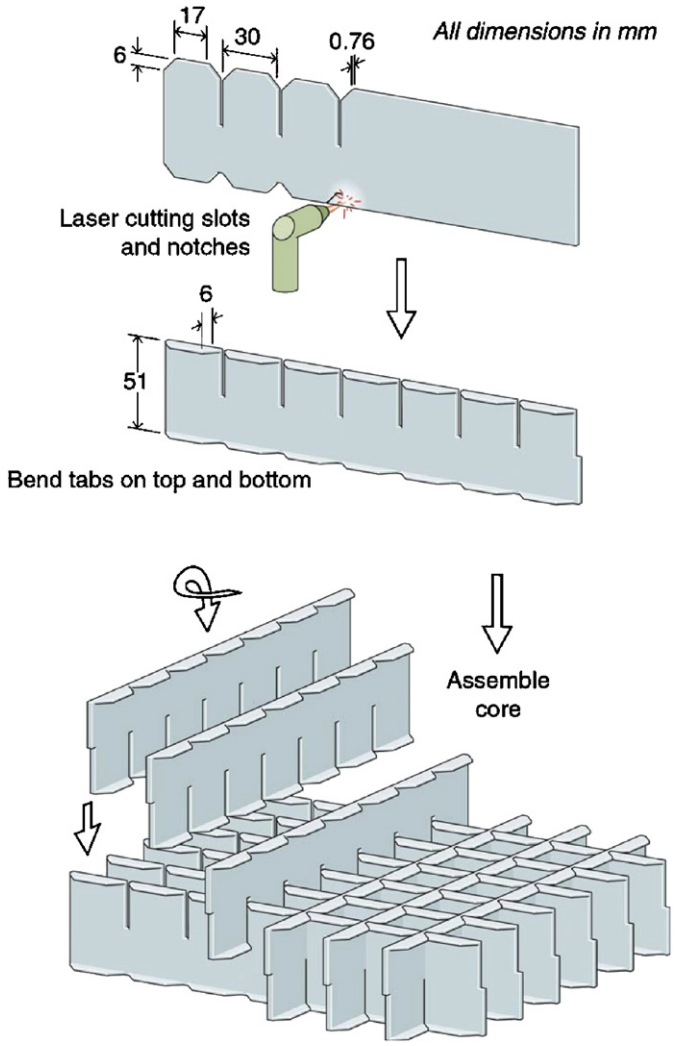

Fig. 5. Square honeycomb core fabrication using a slotted assembly approach.

calculated equivalent solid plate thickness (t_s) was found to be 13.1 mm, and for the baseline solid plate experiments, a 12.7 mm thick solid plate was used.

The square honeycomb core and face sheet were fabricated from a high-ductility stainless steel alloy with an approximate composition of 49Fe–24Ni–21Cr–6Mo (wt%). A slotted metal sheet assembly approach was used for fabrication. Fig. 5 schematically illustrates the fabrication sequence. First, a two-dimensional profile was generated with a laser on a sheet metal strip incorporating the slots needed for the interlocking strip assembly and with allowances for bending the top and bottom flanges. The flanges were then bent at 90 degrees to the core web. Finally, the core was assembled by slip fitting the laser cut and bent strips to form a square grid pattern. The core consisted of an assembly of 38, 0.76 mm thick (22 gauge) strips spaced 30 mm apart to form an 18 cell × 18 cell square grid. A brazing method was used for bonding the face plates to the core. One side of each face plate was sprayed with Wall Colmonoy Nicrobraz 31 braze alloy powder. Three $610 \times 610 \times 61$ mm square honeycomb panel assemblies were then brazed in a vacuum furnace (Solar Atmospheres, Souderton, PA). The furnace chamber was evacuated to a pressure of 0.133 Pa and the temperature was raised to 550 °C and held for approximately 30 min to remove the polymer binder used with the braze alloy. The temperature was then raised to 925 °C at 5 °C/min and the temperature was allowed to equilibrate for 30 min. The temperature was then raised at 3 °C/min to the brazing temperature of 1155 °C and held for 60 min, before cooling to ambient.

4. Air blast experiments

As indicated by equation (3), selection of an explosive charge mass (m) and/or standoff distance (r) enables a test panel to be subjected to a range of blast load intensities. We chose to fix the standoff distance, r, and vary the intensity of loading by varying the explosive charge weight. Three experiments with center detonated, TNT cylindrical charges of 1, 2 and 3 kg at a standoff distance of 10 cm were conducted with the sandwich panel test samples. An identical set of explosive charges was also used for three solid plate tests whose areal density was very close to that of the sandwich panels.

For each test, a cylindrical charge with a length to diameter aspect ratio close to 1 was mounted on a platform with its axis aligned with the center of the test panel. Its front was 10 cm from the front face of the sandwich plate, Fig. 6. Each test sandwich panel or plate was attached to

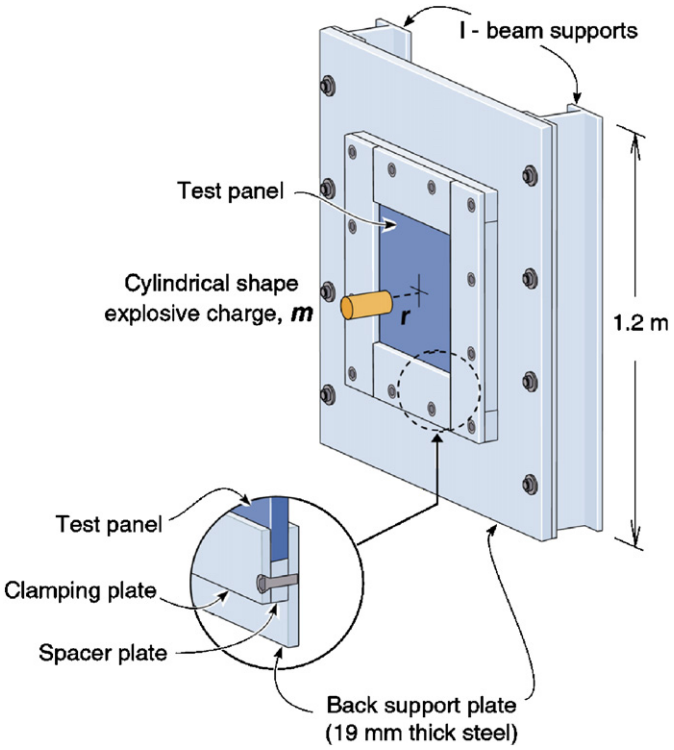

Fig. 6. Schematic arrangement for air blast test.

a 19 mm thick steel plate that was bolted onto two I-beam vertical channels. The I-beam channels were restrained from movement by a heavy back support structure. The 19 mm thick steel support plate had a 410 × 410 mm square hole cut out at the center to allow open space for the sandwich panel to deform. The 610 × 610 × 60 mm sandwich panel was placed vertically against the flat plate, centered on the flat plate opening. A square frame consisting of four flat bars and four 51 × 51 mm square tubes were used to hold the test panel in position. The square tubes were used as spacers between the flat bar frame and the panel support plate. In the test arrangement used, the flat bar strips providing the picture frame effect in

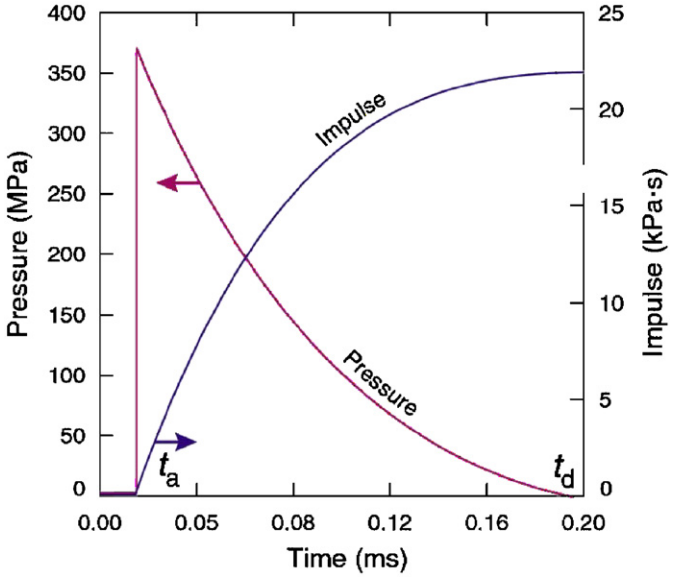

Fig. 7. Reflected pressure and impulse response for an air blast for a 1 kg TNT charge and 0.1 m standoff distance.

Table 1
Peak reflected pressure and reflected impulse calculated from ConWep blast simulation code

Test panel	Peak pressure (MPa)	Impulse (kPa s)
1	366	21.5
2	458	28.4
3	506	33.7

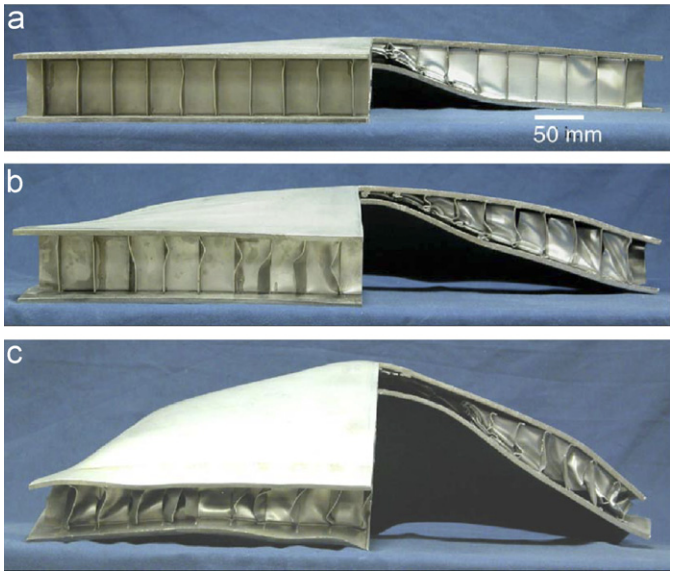

Fig. 8. Half sectioned square honeycomb core test panels: impulse load is (a) 21.5 kPa s, (b) 28.4 kPa s and (c) 33.7 kPa s.

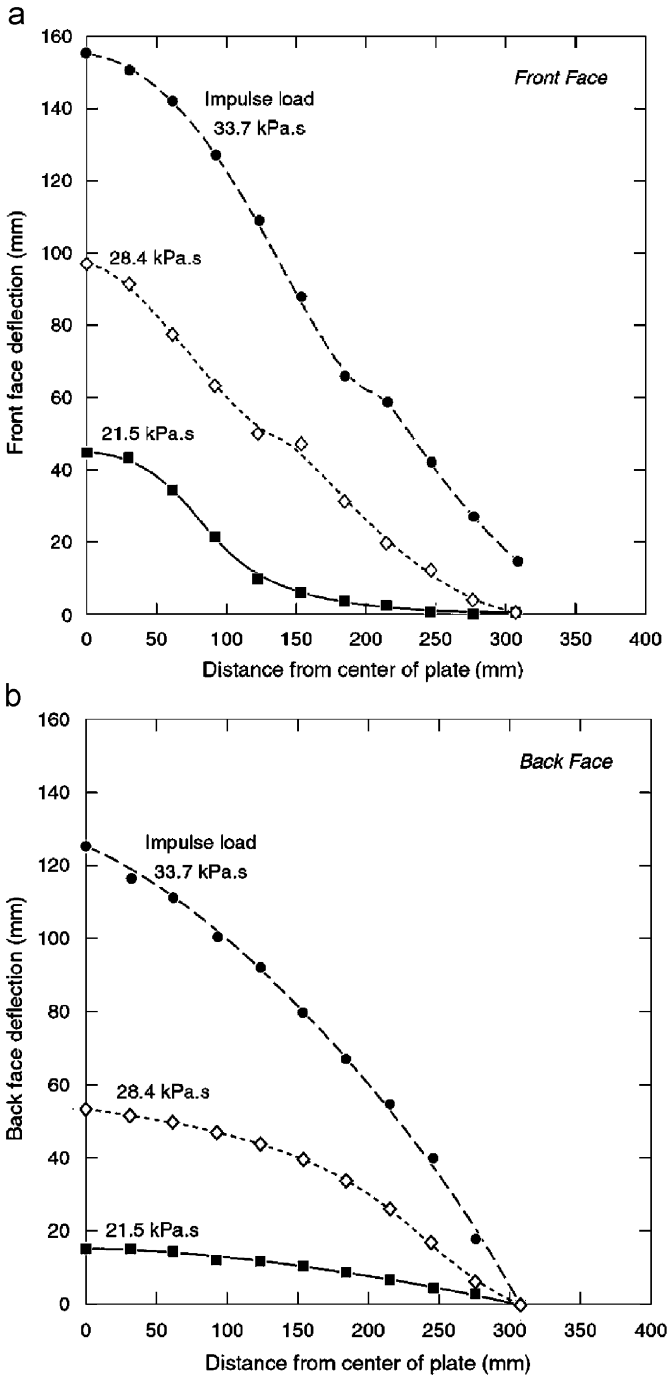

Fig. 9. (a) Front face sandwich panel profile measurements. (b) Back face sandwich panel profile measurements.

front of the test panel were bolted to the back support plate and the bolts tightened to a 34 N m torque level. The process of test panel assembly, explosive charge placement and detonation was repeated for each sandwich panel and solid plate. A quadrant of each panel was wire EDM cut after the explosion tests to examine the deformation mechanisms at the center of each panel.

5. Results

By specifying charge weight, standoff distance and target panel surface area as input information, the ConWep blast simulation code [8] could be used to calculate the spatial distribution of the pressure and impulse loading on a target surface. Although ConWep assumes a spherical air burst or a hemispherical-shaped surface burst adjacent to a reflecting ground plane, we feel that with our center detonated, nearly 1:1 aspect ratio cylindrical charges, it provides a reasonable "estimate" of the pressure loading. Fig. 7 shows the reflected pressure and impulse load response at 10 cm for the 1 kg TNT charge calculated from ConWep. The reflected pressure (which is the "effective" loading on the structure) was found to be ~12 times larger than the incident pressure for this standoff distance and explosive charge, as well as for the 2 and 3 kg charges. Table 1 shows the peak reflected pressures and impulse loads.

Fig. 8 shows the wire EDM cut sandwich panels after the explosion tests. It clearly illustrates the degree of face sheet bending/stretching and core crushing at each impulse load level. In Fig. 8(a), the honeycomb core is only partially crushed at the lowest intensity load. At the next intensity load (Fig. 8b), the core at the center of the panel is completely crushed. Fig. 8c shows that at highest intensity load, core debonding from the front face plate occurred, resulting in a greater separation between the front and back plates (compared with the mid-level intensity loaded panel) indicative of a "spring back" effect of the front plate.

Measurements of the sectioned half profiles are plotted in Fig. 9 for the sandwich panels and in Fig. 10 for the equivalent areal density (12.7 mm thick) solid plates tested at the same impulse load levels. The difference in the front plate (Fig. 9a) and back plate deflections (Fig. 9b) along the length (or width) of the sandwich panel gives a measure of the relative core crushing effect of the square honeycomb core. Core strains of 59% and 87% are deduced from the relative deflections of the front and back face plates for

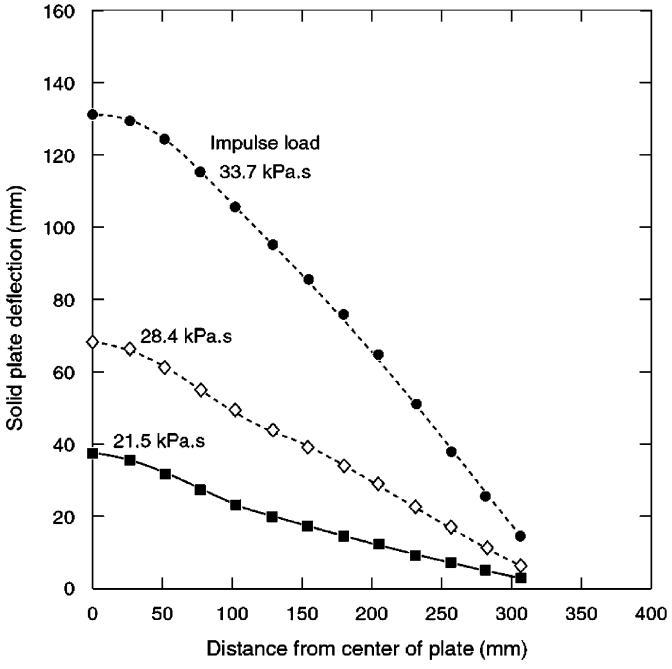

Fig. 10. Solid plate profile measurements.

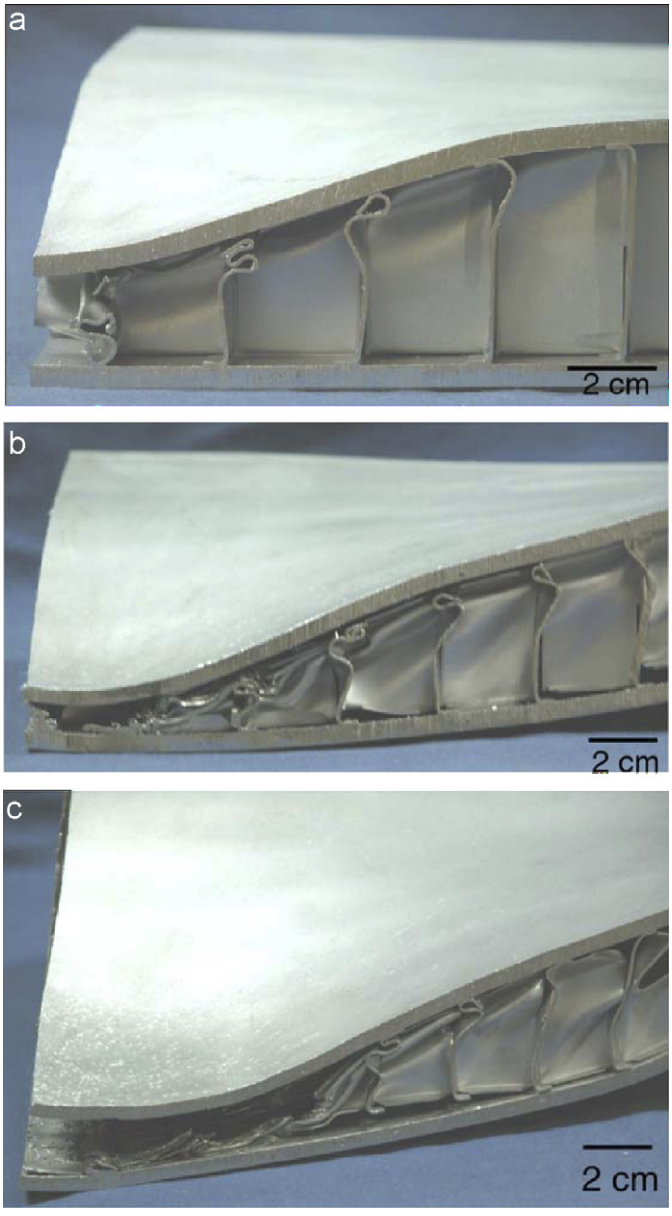

Fig. 11. Cross-sections of square honeycomb cores showing core crushing, cell wall folding: impulse load is (a) 21.5 kPa s, (b) 28.4 kPa s and (c) 33.7 kPa s.

the 21.5 and 28.4 kPa s load intensities. A higher densification strain occurred for the 33.7 kPa s impulse, consistent with the flattened appearance of the core at the center of the panel.

The failure mechanisms of the square honeycomb core under the dynamic loading conditions can be observed from the cross-sections shown in Fig. 11. In Fig. 11(a), cell wall buckling is predominantly observed. A progressive transition from elastic buckling and plastic buckling to cell wall folding (with an increasing number of folds) is clearly seen moving from the outer edge to the center of the panel. Figs. 11(b) and (c) show transverse shear behavior of the core and face sheet stretching with the appearance of core shear bands. Fig. 11(c) also shows a core debonding effect at very high intensity loads.

6. Numerical simulations

Air blast tests are one way of understanding the performance of sandwich panels under dynamic load conditions. Present-day finite element codes allow simulations under these dynamic conditions to be performed without the need for destructive air blast experiments [22,23].

Three-dimensional dynamic finite element calculations were performed using ABAQUS/Explicit [20] to simulate the tests. The faces of the sandwich panels were fully meshed using eight-node linear brick elements with reduced integration. Such elements are capable of accurately capturing the stresses and strains. Each face sheet was discretized with five layers of elements through the thickness. The honeycomb core members were meshed using four-node shell elements with finite membrane strains. Five section integration points with Simpson's integration rule were used in each shell element. These elements allow large rotations and finite membrane deformation, making them particularly well suited for post-buckling analyses. Thirty layers of elements were uniformly distributed through the core thickness. As schematically shown in Fig. 12, the core webs were "welded" to the face sheet at their connections. Support structures were simply modeled as rigid surfaces and the front and back faces of the sandwich panels were assumed to be "welded" to the corresponding rigid wall at all ends. Effects of the contact between the core cell wall and the face sheets due to the plastic buckling, as well as the self-contact of the core wall due to cell wall folding, were taken into account in the model. The contact was taken to be frictionless. A failure criterion was not included in the calculations, so neither fracture of the plate nor core debonding from the front face was captured. Pressure was applied on the surface of the front face as time varying and spatially distributed functions from calculations made with ConWep for the explosive material, charge weight and standoff distance values used for the experiment. Although ConWep assumes a spherical air blast (and not a cylindrical charge), it is believed that with center detonated cylindrical charges with length to diameter aspect ratios close to 1, it provides a reasonable estimate of the blast wave pressure loading profile. For any point on the surface of the front face, its distance to the center of the front face surface is noted as d, and then the pressure on that point can be expressed as a function of d and t, such that

$$p(d,t) = p(t)\,\mathrm{e}^{-(d/d_0)^2}, \tag{7}$$

where d_0, the reference distance, is determined by fitting the results from calculations made with ConWep, and $p(t)$ is given by Eq. (2). Fig. 13 shows that, when d_0 is set as 0.12 m for all levels of applied impulses, Eq. (7) provides very good estimates of peak pressure applied to the panel for the whole range of distance from the center to any location of interest. Finally, because of the symmetry of the structure and loading condition, only one quarter of the panel was analyzed for simplification, where the symmetry boundary conditions were imposed to the sandwich panel as illustrated in Fig. 12.

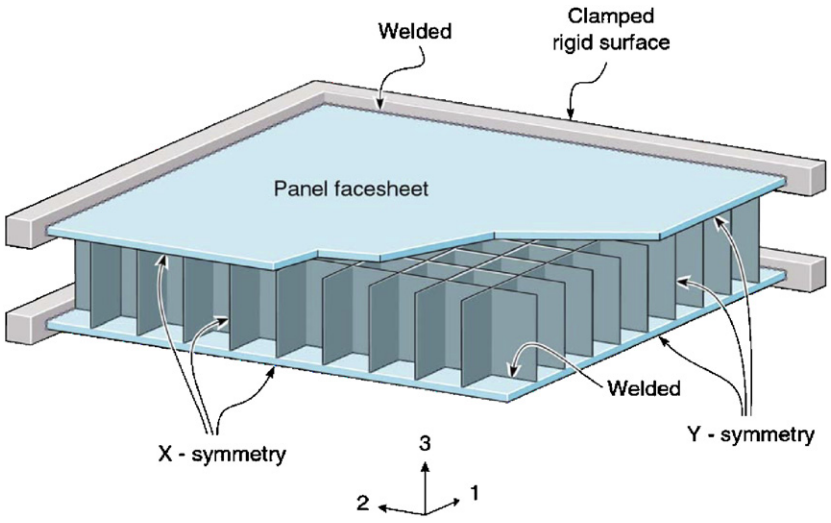

Fig. 12. Schematic diagram of the finite element model geometry (1/4th of geometry modeled due to symmetry).

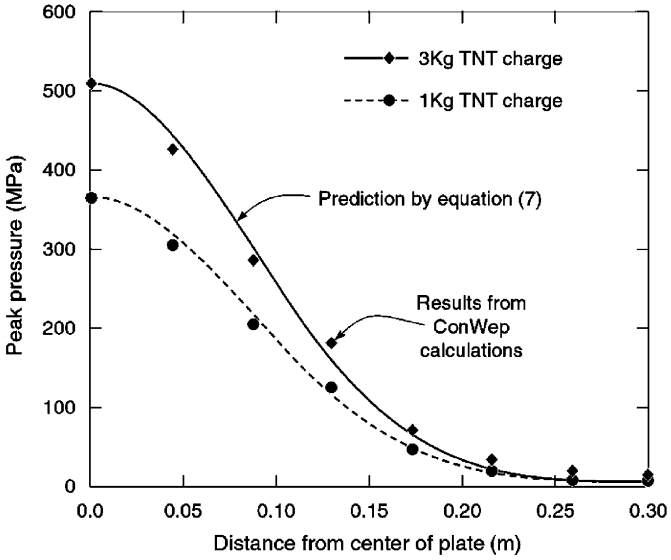

Fig. 13. Spatial distributions of peak pressure exerted on the surface from 1 and 3 kg TNT explosions at a 0.1 m standoff distance.

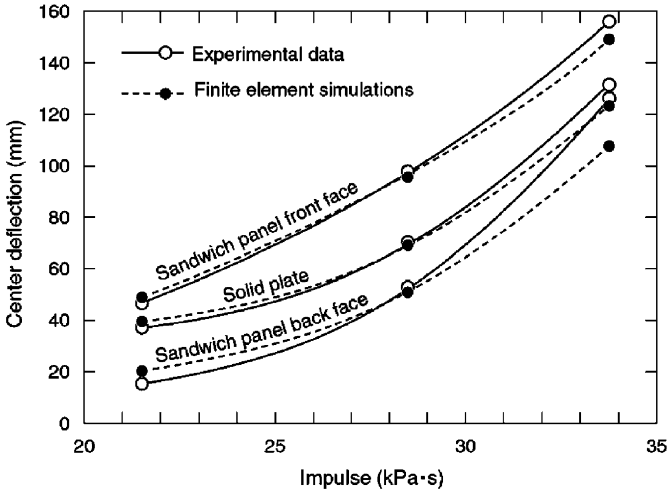

Fig. 14. Measurements and simulations of panel deflections after "spring back" as a function of impulse loading. The deflections of the front and back faces of the sandwich panel are compared with the solid plate center deflections.

Simulations were carried out with strain rate dependence for the stainless steel alloy. This material has substantial strain hardening that is nearly linear and moderate strain rate sensitivity. In tension, the relation between true stress and true strain is taken to be strictly bilinear for each value of plastic strain rate, $\dot{\varepsilon}_p$, as

$$\sigma = \begin{cases} E\varepsilon, & \varepsilon \leqslant \dfrac{\sigma_Y}{E}\left(1+(\dot{\varepsilon}_p/\dot{\varepsilon}_0)^m\right), \\ \sigma_Y\left(1+(\dot{\varepsilon}_p\dot{\varepsilon}_0)^m\right)+E_t\left(\varepsilon-\dfrac{\sigma_Y}{E}\left(1+(\dot{\varepsilon}_p/\dot{\varepsilon}_0)^m\right)\right), & \varepsilon > \dfrac{\sigma_Y}{E}\left(1+(\dot{\varepsilon}_p/\dot{\varepsilon}_0)^m\right). \end{cases} \tag{8}$$

Here, Young's modulus $E = 200$ GPa, Poisson's ratio $v = 0.3$, initial yield stress $\sigma_Y = 300$ MPa and tangent modulus $E_t = 2.0$ GPa. Dynamic measurements on stainless steels are well represented using the values $\dot{\varepsilon}_0 = 4916\,s^{-1}$ and $m = 0.154$ [15,24].

Additional three-dimensional finite element calculations were performed for equivalent mass solid plates and the results are presented in Section 7. The solid plates were fully meshed using eight-node linear brick elements with reduced integration. The material properties and boundary conditions were similar to those imposed on the sandwich panels.

7. Discussion

Fig. 14 shows the center deflections of the sandwich panel front face, back face and the equivalent solid plate plotted as a function of the impulse load. The finite element-predicted deflections after panel spring back are also plotted for comparisons with the experimental measurements. The benefits of a sandwich panel construction over a solid plate to withstand blast loads are clearly evident by the lower back plate deflections compared with the equivalent weight solid plates subjected to the same loads. The benefits of sandwich construction are particularly evident at low impulse levels ($I = 21.5$ kPa s), wherein the center deflection of the back face is only about 40% of those for the solid plate. At high impulse levels ($I = 33.7$ kPa s), the benefits diminish, the deflections of the sandwich panel being about 90% of the solid panel.

Figs. 15(a)–(c) illustrate deformed sandwich panels for each impulse load level predicted by finite element simulations. Compared with the corresponding experimental measurements and observations (Fig. 8), the simulations capture most of the details of the deformation patterns quite realistically, including shearing of the core and buckling of the lateral webs. Moreover, the center displacements deduced from the calculations, when superposed on Fig. 14, are very similar to the measurements for both sandwich panel and equivalent solid plate at two lower impulse levels ($I = 21.5$ and 28.4 kPa s). It is noticeable in Fig. 8(c) that the highest intensity load results in a separation between the front face and core webs, thus weakening the overall strength of the plate, while the present finite element model does not capture this failure mechanism since a debonding criterion was not included. Additionally, the edges of the sandwich panel used with the test arrangement are actually more "flexible" than the "clamped" condition that was adopted in the present finite element simulation. Consequently, the finite element simulation predicts a smaller center deflection for the sandwich panel, and also for the solid plate for the highest impulse level ($I = 33.7$ kPa s) as plotted in Fig. 14.

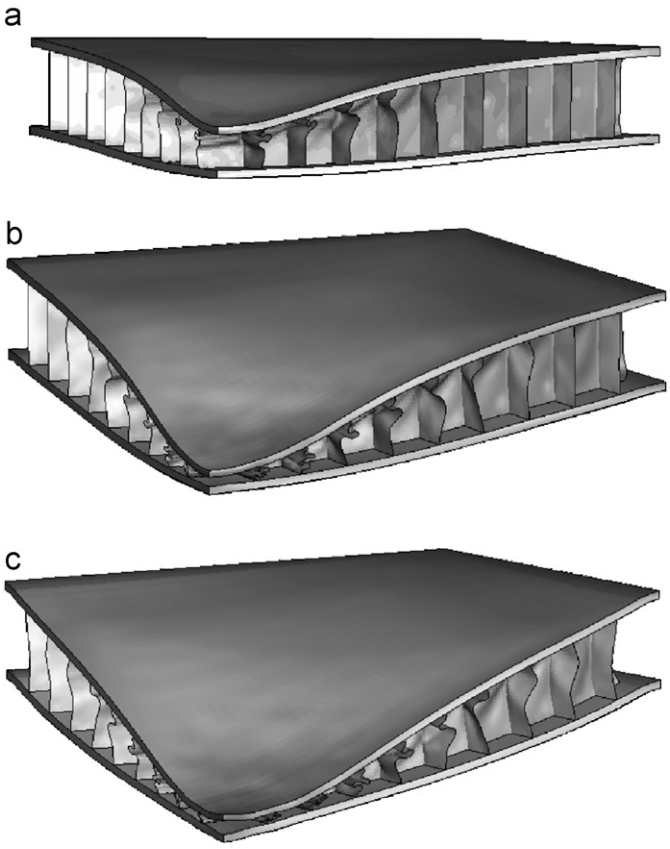

Fig. 15. Finite element simulations of the sandwich panel deformation at impulse levels (a) 21.5 kPa s, (b) 28.4 kPa s and (c) 33.7 kPa s.

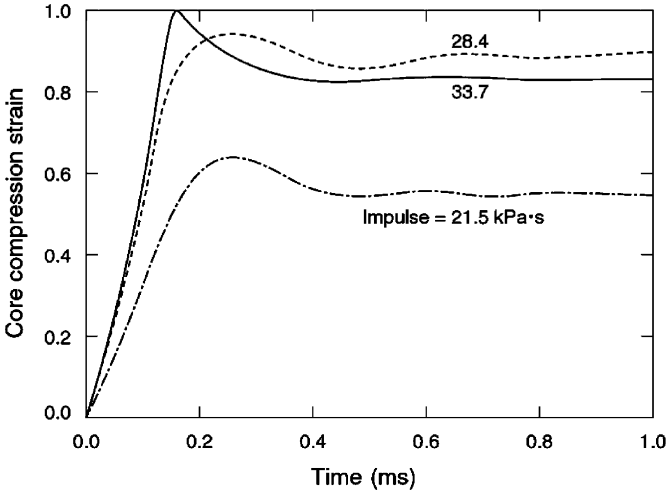

Fig. 16. Time dependence of core crushing obtained from finite element calculations.

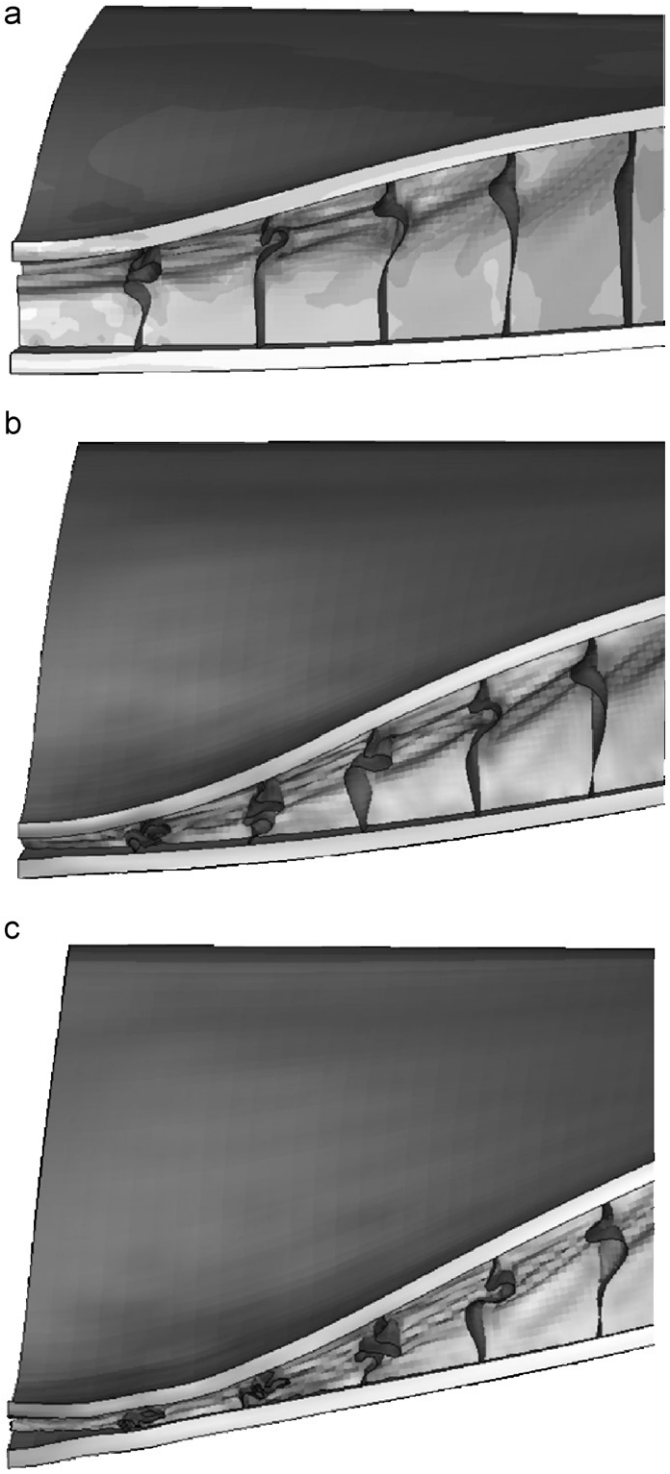

Fig. 17. Finite element simulations of core crushing and transverse shear behavior near the center of the panels, at impulse levels (a) 21.5 kPa s, (b) 28.4 kPa s and (c) 33.7 kPa s.

Computed core compressive strains at the center of the panel as a function of time for each applied impulse are shown in Fig. 16. Significant core crushing occurs for high intensity impulses. For example, the maximum core compressive strain is up to 1 for the highest impulse ($I = 33.7$ kPa s). It is also indicated that core web crushing has been completed very quickly, within a time less than 0.2 ms, followed by a "spring back" phenomenon of core compression strain. Particularly, the "spring back" effect for the highest impulse ($I = 33.7$ kPa s) is more obvious than that for moderately high impulse ($I = 28.4$ kPa s), which is again consistent with the experimental observations.

The effects of impulse on the mode of core crushing are also illustrated in the close up view of the FEM-predicted panel deformed shape shown in Fig. 17. All three longitudinal core members near the sandwich panel center buckle plastically. The crushing strains are greatest in the central core member, because of the greatest applied pressure associated with the explosion. For the lowest impulse ($I = 21.5\,\text{kPa s}$), the buckle of the core web is located within the upper segment of the core member, whereas the lower segment remains planar and undeformed. This is consistent with the previous finding on the dynamic crush behavior of square honeycomb sandwich cores by Xue and Hutchinson [14]. In Fig. 17, the extensive bending of the buckled segment causes it to contact the front face. Correspondingly, the associated plastic strain ruptures the contact node as shown in Fig. 11. Good agreement is observed between the finite element predicted and experimental panel deformed shapes, except for the observation that the present finite element model fails to predict the debonding of core webs. For example, at the intermediate intensity load level (Fig. 17b), evidence of core shear is indicated by the appearance of shear bands also observed in the experimentally tested panel (Fig. 11b). At the highest load (Fig. 17c), complete crushing of the core is predicted, which is consistent with experimental observations (Fig. 11c).

For the intermediate intensity load ($I = 28.4\,\text{kPa s}$), the overall stretching forces of the front face and back face of the sandwich panel along one edge are plotted as a function of time in Fig. 18. In the present finite element model, forces can be calculated as the reaction forces exerted on the corresponding support structures modeled as rigid surfaces. Because of the symmetry of the structure and loading condition, all four sides have almost the same force responses. When the sandwich panel deforms, the front face starts to stretch very early, then the stretching force remains at a high level, and finally the stretching force is released. While the back face is under compression first, where bending dominates the overall behavior of the sandwich panel, the back face starts to stretch at around 0.3 ms, and finally the stretching force of the back face is also released. The maximum stretching force experienced at the front face is twice that at the back face, thus indicating that the front face is much easier to fail.

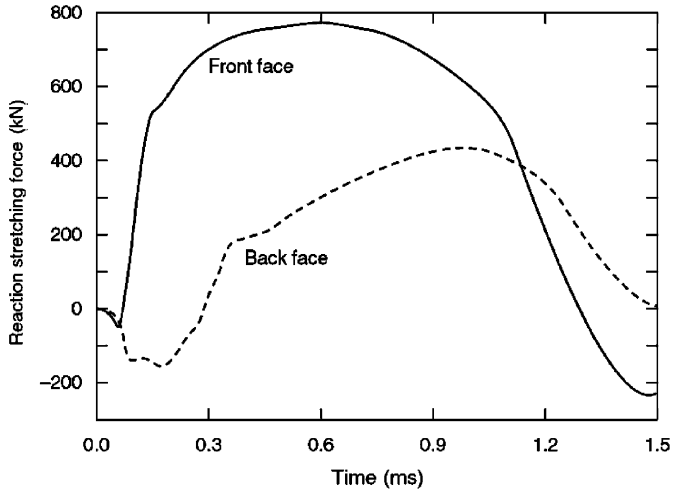

Fig. 18. Overall stretching forces exerted on the support structures on one side of the sandwich panel.

8. Conclusions

From the series of basic experiments conducted in this study, the advantage of using a sandwich structure with a cellular metal core has been demonstrated as a suitable candidate for deflection-limited designs capable of withstanding air blast loads. A more detailed experimental study with well-established boundary conditions (e.g. clamped edges) and different face sheet selections is needed to fully realize the face sheet stretching contribution to the overall blast energy absorption and sandwich panel performance. Finite element simulations of the air blast loading on the test panels have been able to capture the phenomenological details of the sandwich panel deformation. A finite element model that incorporates a debonding failure criterion of the face sheet–core interface is needed to analyze this mode of failure, which appears to be important for higher intensity blasts.

Acknowledgments

We wish to thank Keith Williams and Mike Maston of NEWTEC services group for their explosive test services, and Christian Yungwirth for his support with the air blast experiments. We also wish to acknowledge Ed Johnson, Steve Fishman and Roshdy Barsoum of the Office of Naval Research for their support of our research in this area. The research described above was conducted under grant number N00014-03-1-0281.

References

[1] Fleck NA, Deshpande VS. The resistance of clamped sandwich beams to shock loading. J Appl Mech 2004;71:386–401.
[2] Xue Z, Hutchinson JW. Preliminary assessment of sandwich plates subject to blast loads. Int J Mech Sci 2003;45:687–705.
[3] Xue Z, Hutchinson JW. A comparative study of impulse-resistant metal sandwich plates. Int J Impact Eng 2004;30:1283–305.
[4] Rathbun HJ, Radford DD, Xue Z, He MY, Yang J, Deshpande VS, et al. Performance of metallic honeycomb-core sandwich beams under shock loading. Int J Solids Struct 2006;43:1746–63.
[5] Hutchinson JW, Xue Z. Metal sandwich plates optimized for pressure impulses. Int J Mech Sci 2005;47:545–69.
[6] Baker WE. Explosions in air. Austin, TX: University of Texas Press; 1973.
[7] Smith PD, Hetherington JG. Blast and ballistic loading of structures. Butterworth-Heinemann: London; 1994.
[8] ConWep blast simulation software, US Army Corps of Engineers, Vicksburg, MS.
[9] Deshpande VS, Fleck NA. Blast resistance of clamped sandwich beams, ICTAM04.
[10] Fleck NA, Deshpande VS. The resistance of clamped sandwich beams to shock loading. J Appl Mech 2004;71:386–401.

[11] Ashby MF, Evans AG, Fleck NA, Gibson LJ, Hutchinson JW, Wadley HNG. Metal foams: a design guide. London: Butterworth-Heinemann; 2000.
[12] Gibson LJ, Ashby MF. Cellular solids: structure and properties. 2nd ed. Cambridge: Cambridge University Press; 1997.
[13] Plantema FJ. Sandwich construction. New York: Wiley; 1966.
[14] Xue Z, Hutchinson J. Crush dynamics of square honeycomb sandwich cores. Int J Numer Methods Eng 2005;65:2221–45.
[15] Nemat-Nasser S, Guo WG, Kihl DP. Thermomechanical response of AL-6XN stainless steel over a wide range of strain rates and temperatures. J Mech Phys Solids 2001;49:1823–46.
[16] Wadley HNG, Fleck NA, Evans AG. Fabrication and structural performance of periodic cellular metal sandwich structures. Compos Sci Technol 2003;63:2331–43.
[17] Kooistra GW, Deshpande VS, Wadley HNG. Compressible behavior of age hardenable tetrahedral lattice truss structures made from aluminum. Acta Mater 2004;52:4229–37.
[18] Wang J, Evans AG, Dharmasena KP, Wadley HNG. On the performance of truss panels with Kagome cores. Int J Solids Struct 2003;40:6981–8.
[19] Queheillalt DT, Wadley HNG. Cellular metal lattices with hollow trusses. Acta Mater 2005;53:303–13.
[20] ABAQUS/Explicit user's manual, Version 6.0, Hibbit, Karlsson and Sorenson Inc., 2001.
[21] Cooper PW. Explosives engineering. New York: Wiley-VCH; 1996.
[22] ChungKimYuen S, Nurick GN. Experimental and numerical studies on the response of quadrangular stiffened plates. Part I: Subjected to uniform blast load. Int J Impact Eng 2005;31(1):55–83.
[23] Langdon GS, ChungKimYuen S, Nurick GN. Experimental and numerical studies on the response of quadrangular stiffened plates. Part II: Localised blast loading. Int J Impact Eng 2005;31(1):85–111.
[24] Stout MG, Follansbee PS. Strain rate sensitivity, strain hardening, and yield behavior of 304 L stainless steel. Trans ASME: J Eng Mater Tech 1986;108:344–53.